



1 **Characterization of black carbon-containing fine particles**
2 **in Beijing during wintertime**

3 Junfeng Wang¹, Dantong Liu², Xinlei Ge^{1*}, Yangzhou Wu¹, Fuzhen Shen¹, Mindong Chen¹, Jian
4 Zhao^{3,4}, Conghui Xie^{3,4}, Qingqing Wang³, Weiqi Xu^{3,4}, Jie Zhang⁵, Jianlin Hu¹, James Allan^{2,6},
5 Rutambhara Joshi², Pingqing Fu³, Hugh Coe² and Yele Sun^{3,4}

6 ¹Jiangsu Key Laboratory of Atmospheric Environment Monitoring and Pollution Control, School of
7 Environmental Science and Engineering, Nanjing University of Information Science and Technology,
8 Nanjing 210044, China

9 ²School of Earth and Environmental Sciences, University of Manchester, M13 9PL, Manchester, UK

10 ³State Key Laboratory of Atmospheric Boundary Layer Physics and Atmospheric Chemistry, Institute
11 of Atmospheric Physics, Chinese Academy of Sciences, Beijing 100029, China

12 ⁴University of Chinese Academy of Sciences, Beijing 100049, China

13 ⁵Atmospheric Sciences Research Center, University at Albany, State University of New York, NY,
14 12203, USA

15 ⁶National Centre for Atmospheric Science, University of Manchester, M13 9PL, Manchester, UK

16

17 *Corresponding author, Email: caxinra@163.com

18 Phone: +86-25-58731394

19

20

21

22

23

24

25 **Abstract**

26 Refractory black carbon (BC) is a product from incomplete combustion of fossil fuel, biomass and
27 biofuel, etc. By mixing with other species, BC can play significant roles in climate change, visibility
28 impairment and human health. Such BC-containing particles in very densely-populated megacities,
29 like Beijing, may have specific sources and properties, that are very important to the haze formation
30 and air quality. In this work, we characterized exclusively the BC-containing particles only in urban
31 Beijing, by using a laser-only Aerodyne soot particle aerosol mass spectrometer (SP-AMS), as a part
32 of the Air Pollution and Human Health (APHH) 2016 winter campaign. The average mass ratio of
33 coating-to-BC (R_{BC}) was found to be ~ 5.0 , much smaller than those of highly aged BC, indicating
34 dominant contributions from primary emissions. Positive matrix factorization indeed shows the
35 dominance of fossil fuel and biomass burning organics. Yet secondary species, including both sulfate,
36 nitrate and oxygenated organic aerosol (OA) species, could have significant impacts on the properties
37 of BC-containing particles, especially for ones with larger BC core sizes and thicker coatings. Analyses
38 of the sources and diurnal cycles of organic coating reveal significant afternoon photochemical
39 production of secondary OA (SOA), as well as the nighttime production of a portion of highly
40 oxygenated OA. Besides SOA, photochemical production of nitrate, not sulfate, was very important.
41 Further investigations on BC-containing particles at different periods show that, on average, more
42 polluted periods would have more contributions from secondary species, and more thickly coated BC
43 tended to associate with more secondary species, indicating the important role of chemical aging to
44 the air pollution in urban Beijing during wintertime. However, for individual pollution events,
45 aqueous-phase production of sulfate, nitrate and SOA might aggravate the pollution obviously under
46 high relative humidity conditions, while sometimes local primary emissions (coal and biomass burning)
47 could lead to serious and extremely polluted event too.

48



49 1. Introduction

50 Black carbon (BC) is generated from incomplete combustion of carbon-based fuels (Ramanathan
51 and Carmichael, 2008), and can exert significant impacts on global and regional climate, planetary
52 boundary layer height (PBLH), air quality and human health, etc. (Lee et al., 2017; Bond et al.,
53 2013; Ding et al., 2016). BC can strongly absorb solar radiation and warm up the atmosphere directly.
54 By internally or externally mix with non-BC materials (coatings, including co-emitted primary
55 organics/inorganics and secondary materials that associate with BC) (Chen et al., 2016a; Lee et al.,
56 2017; Wang et al., 2017a), the properties and morphologies of BC might be altered greatly (Liu et al.,
57 2013; Liu et al., 2017; Liu et al., 2015; Cappa et al., 2012; Peng et al., 2016). Thick coating can increase
58 the mass absorption cross section of BC, thus enhance the light absorption of BC core via “lensing
59 effect” (Jacobson, 2011; Liu et al., 2015; Pokhrel et al., 2017). However, coating thickness of BC-
60 containing particles significantly depends on their sources/chemical composition and aging processes,
61 thus there are great uncertainties on light absorption enhancement (E_{abs}) of BC as well as its global
62 radiative forcing (Cappa et al., 2012; Liu et al., 2017; Cui et al., 2016; Liu et al., 2015). For instance, the
63 mass ratio of coatings to BC core (R_{BC} , an analog of coating thickness) from biomass burning is usually
64 greater than 3 (Liu et al., 2017) and can be larger than 10 in remote sites (Wang et al., 2017a). Normally,
65 when R_{BC} is less than 1.5, it is probably from traffic sources, whereas secondary organic aerosol (SOA)
66 dominated BC-containing particles is usually with a R_{BC} greater than 4 (Lee et al., 2017). Moreover,
67 the coating species can modify the hygroscopicity of BC-containing particles (Liu et al., 2013) when
68 associated with hydrophilic materials, and some of them can serve as cloud condensation nuclei (CCN),
69 therefore alter the albedo and precipitation of clouds indirectly (Dusek et al., 2010; Dusek et al., 2006).

70 In the past decades, a number of field studies on BC have been conducted in the winter of Beijing,
71 and mainly focused on BC mass loadings, mixing states, optical properties, human health impacts and
72 sources (coal combustion, biomass burning and vehicles, etc.) (Wu et al., 2017; Cheng et al., 2017; Ji
73 et al., 2017; Wang et al., 2017b; Wu et al., 2016; Chen et al., 2016b; Meng et al., 2016; Wang et al.,
74 2016b; Liu et al., 2016; Yang et al., 2014; Schleicher et al., 2013a; Schleicher et al., 2013b; Song et al.,
75 2013; Zhang et al., 2017). There were real-time studies on BC, and on the chemical characteristics of
76 total fine particles (including particles with and without BC) in Beijing. However, to the best of our
77 knowledge, no study was conducted in real-time to characterize exclusively only BC-containing
78 particles in Beijing despite the important effects of coating materials on BC properties aforementioned.



79 Currently, a few studies have explored BC-containing particles in other locations, e.g., Toronto (Willis
80 et al., 2016; Lee et al., 2015), California (Lee et al., 2017; Massoli et al., 2015; Cappa et al., 2012),
81 London (Liu et al., 2015) and Tibet (Wang et al., 2017a) by using the Aerodyne soot-particle Aerosol
82 Mass Spectrometer (SP-AMS) (Onasch et al., 2012; Lee et al., 2015; Wang et al., 2016a; Ge et al.,
83 2017b). The SP-AMS physically combines the 1064 nm laser vaporizer of single particle soot
84 photometer (SP2) into a high-resolution aerosol mass spectrometer (HR-AMS) (Onasch et al.,
85 2012; Canagaratna et al., 2007). After removal of the AMS tungsten vaporizer and by operating the
86 instrument with the laser vaporizer only, refractory BC as well as its associated coating can be
87 evaporated since the 1064 nm laser can selectively heat the BC (Massoli et al., 2015). In other words,
88 the laser-only SP-AMS can exclusively measure BC cores and the species coated on BC cores. This
89 unique technique allows us to explore in details the characteristics of BC-coating species with no
90 perturbations from other co-existing non-BC containing particles in ambient air.

91 Beijing, as the most reprehensive megacity with a large population in developing countries, the
92 BC-containing particles may have specific source profiles and physiochemical properties, therefore
93 elucidation of its characteristics is important to understand the haze formation and improve air quality
94 in such regions. In this work, we report for the first time the real-time measurement results on the
95 chemical composition, mass loading, size distribution, and sources/processes of the BC-containing
96 particles during wintertime of 2016 in urban Beijing by using the laser-only SP-AMS. Results
97 regarding mixing states and optical properties are presented in other publications in this special issue.

98

99 2. Experiments

100 2.1 Sampling site and instrumentation

101 As a part of the UK-CHINA Air Pollution & Human Health (APHH) winter campaign, we
102 conducted measurements at the Tower Division of Institute of Atmospheric Physics (IAP), Chinese
103 Academy of Science (39°58'N, 116°22'E) in Beijing (Figure S1 in the supplement), from 15 November
104 to 13 December of 2016. The site was surrounded by residential infrastructures and a freeway in the
105 east (360m).

106 The SP-AMS was deployed on the rooftop of Herong Building (~8m above the ground), with a
107 PM_{2.5} cyclone (Model URG-2000-30EN) and a diffusion dryer in front of the inlet. The single particle
108 soot photometer (SP2, Droplet Measurement Technology, Inc., Boulder, CO, USA) was operated



109 simultaneously nearby inside another container (~20 m away) on the ground. The SP2 incandescence
110 signal was calibrated for BC mass by using Aquadag® black carbon standard (Aqueous Deflocculated
111 Acheson Graphite, Acheson Inc., USA) (Laborde et al., 2012). For the SP-AMS, since the filament
112 that ejects electrons can still heat the tungsten vaporizer up to ~200 °C (Willis et al., 2014) even it is
113 turned off, the tungsten vaporizer was thus physically removed to make sure only BC and its associates
114 were vaporized by the laser, and to eliminate influences from species uncoated on the BC cores.

115 The tuning and calibration procedures of the SP-AMS followed the procedures described
116 previously (Lee et al., 2015; Willis et al., 2016; Massoli et al., 2015; Wang et al., 2017a). During the
117 campaign, the SP-AMS was run with a 10-minutes cycle: one W mode with high chemical resolution
118 (2.5 min) and two mass sensitive V modes including one with particle time of flight (PToF) mode (2.5
119 min) and another one (5 min) with the measured m/z up to 2000 to investigate fullerene-like carbon
120 clusters (Wang et al., 2016a). The filtered air measurement was performed for a day to determine the
121 detection limits (DLs) of various aerosol species and to adjust the fragmentation table. The ionization
122 efficiency (IE) and relative ionization efficiency (RIE) of sulfate and nitrate were calibrated by using
123 pure ammonium nitrate and ammonium sulfate according to Jayne et al. (2000), respectively. RIE of
124 BC was calibrated by using Regal Black (RB, REGAL 400R pigment black, Cabot Corp.) (Onasch et
125 al., 2012), and the average ratio of C_1^+ to C_3^+ was determined to be 0.53 to minimize the influence of
126 C_1^+ from non-refractory organics. However, it should be aware that laser-only SP-AMS cannot
127 vaporize ammonium nitrate/sulfate if they do not coat on BC, thus the IE and RIE calibrations were
128 done before removal of the tungsten vaporizer and the values were assumed to be unchanged after the
129 tungsten heater's removal (Willis et al., 2016). Note the RIE of BC was calibrated before the campaign
130 and was repeated in the middle and end of the campaign. RIEs of nitrate, ammonium, sulfate and BC
131 were determined to be 1.1, 3.82, 0.82, and 0.17, respectively. The default value of 1.4 was used as RIE
132 of organics (Canagaratna et al., 2007). Polystyrene latex (PSL) spheres (100-700 nm) (Duke Scientific
133 Corp., Palo Alto, CA) were used to calibrate the size before the campaign (Canagaratna et al., 2007).

134 **2.3 Data Analysis**

135 Standard AMS data analysis software (Squirrel and Pika) based on Igor Pro 6.37 (Wavemetricks,
136 Lake Oswego, OR, USA) were used to obtain the concentrations, mass spectra and size distributions
137 of BC and its coating species. All data were calculated based on high-resolution fitting results. Due to
138 different vaporization schemes between the SP-AMS and HR -AMS, mass spectra from these two



139 instruments even for the same population of particles are not entirely the same. Laser-only SP-AMS
140 can result in overall less fragmentation, therefore the mass profile may contain more large m/z
141 fragments and less small m/z fragments compared with that from HR-AMS (Massoli et al., 2015).
142 Therefore, here the elemental ratios of organics, i.e., oxygen-to-carbon, hydrogen-to-carbon and
143 nitrogen-to-carbon ratios (O/C, H/C and N/C) were determined by the Aiken approach first (Aiken et
144 al., 2008), and then O/C and H/C were corrected by using factors of 0.83 and 1.16, respectively
145 (Canagaratna et al., 2015).

146 Source apportionment for organics coated on BC was conducted by using Positive matrix
147 factorization (PMF) (Paatero and Tapper, 1994) Evaluation Tool written in Igor (Ulbrich et al., 2009).
148 In this study, high-resolution mass spectra (HR-MS) of organic (including BC) and inorganic species
149 were combined together to perform the PMF analyses (Sun et al., 2012; Wang et al., 2017a; Wang et al.,
150 2018). It should be noticed that, only fragment ions from polycyclic aromatic hydrocarbons (PAHs)
151 were included for m/z range of ~ 150 to ~ 250 in the PMF analysis because of the limited mass resolution
152 of SP-AMS. All PMF solutions were evaluated following the standard instruction (Zhang et al., 2011).
153 Finally, four types of organic aerosol (OA) associated with BC were determined eventually, including
154 a fossil fuel combustion OA (FFOA), a biomass burning OA (BBOA) and two oxygenated OA (OOA1
155 and OOA2).

156 Supporting data such as meteorological parameters including relative humidity (RH), wind speed
157 (WS), wind direction (WD) and temperature (T), as well as concentrations of gaseous species such as
158 O₃, SO₂, NO, NO₂, NO_x, NO_y, NO_z, and CO were measured in parallel simultaneously. All data
159 reported here were at local time (Beijing Time, UTC+8).

160

161 **3. Results and discussions**

162 **3.1 Overview of BC-containing aerosol characteristics**

163 Figs. 1 and 2 show the temporal variations of meteorology parameters, mass loadings of gaseous
164 pollutants (CO, NO_x, SO₂ and O₃), BC and its associated coating components (sulfate, nitrate,
165 ammonium, chloride, total OA and the four PMF-resolved OA factors). The campaign-averaged
166 composition of BC-containing particles and mass contributions of the four OA factors to total OA were
167 also displayed in Fig. 2. Overall, wind directions and speeds had close associations with the overall
168 mass loadings of BC-containing particles. The pollution periods (characterized by concentrations of



169 BC-containing particles above $10 \mu\text{g m}^{-3}$) were accompanied by low wind speeds ($<4 \text{ m s}^{-1}$) and in a
170 relatively large part from southern air masses since Beijing is at the foot of the mountains which
171 facilitate the accumulation of pollutants from southern North China Plain (NCP). The clean periods
172 (characterized by the concentrations of BC-containing particles below $10 \mu\text{g m}^{-3}$) were mainly under
173 the control of strong winds ($>4 \text{ m s}^{-1}$) from the northwest. During the campaign, the mass loadings of
174 BC cores and BC-containing particles ranged from $0.11 \sim 26.54 \mu\text{g m}^{-3}$ and $0.71 \sim 174.40 \mu\text{g m}^{-3}$, with
175 an average of $4.9 \mu\text{g m}^{-3}$ and $29.4 \mu\text{g m}^{-3}$, respectively. We also compared BC concentrations
176 determined by the SP-AMS with those from SP2, and they correlated quite well with each other (r^2 of
177 0.93; Fig. S3), indicating the quantification of BC by the SP-AMS is reliable.

178 The coating species occupied on average about 83.4% of the mass of BC-containing particles,
179 indicating BC was generally thickly coated throughout the whole campaign, with an average mass
180 ratio of coatings to BC (R_{BC}) of ~ 5 . Organic aerosol (OA) was the most abundant coating component,
181 taking up to 59.4% of the total mass, followed by nitrate, sulfate, ammonium and chloride (8.8%, 6.5%,
182 4.7% and 4.0%, respectively). OA correlated quite well with BC (r^2 of 0.97), suggesting that many OA
183 species were co-emitted and mixed with BC, and indeed, primary OA (POA=FFOA+BBOA) was
184 found to dominate the OA mass ($66.3\%=43.9\%+22.4\%$). Chloride (Cl) had a great correlation with
185 BC (r^2 of 0.94), suggesting it was mainly associated with primary emissions, for example, gasoline,
186 diesel and coal combustion during wintertime in urban Beijing. Sulfate and nitrate are typically
187 secondarily formed, therefore their correlations with BC were relatively weak (r^2 of 0.64 for SO_4^{2-} vs.
188 BC, and 0.60 for NO_3^- vs. BC). Their properties are discussed in more details in the following sections.

189

190 3.2 Chemically-resolved size distributions of BC-containing particles

191 Fig. 3a shows the campaign-averaged mass-based size distributions of major BC-coating species,
192 including organics (BC-Org), sulfate (BC-Sulfate), nitrate (BC-Nitrate), chloride (BC-Chl) and BC
193 core itself. It should be noticed that the size distribution of BC was scaled from that of m/z 24 (C_2^+),
194 as other major carbon cluster ions might be significantly affected by other ions, for example, C_1^+ at
195 m/z 12 can be influenced by fragments from non-BC organics, C_3^+ at m/z 36 by HCl^+ , C_4^+ at m/z 48 by
196 SO^+ , and C_5^+ at m/z 60 by $\text{C}_2\text{H}_4\text{O}_2^+$ etc. Similarly, the size distribution of BC-Chl was scaled from Cl^+
197 signal at m/z 35. As shown in Fig. 3a, on average, size distributions of BC-Sulfate, BC-Nitrate and BC-
198 Org displayed a similar pattern with a major peak at $\sim 550 \text{ nm}$ (vacuum aerodynamic diameter, D_{va}),



199 suggesting that they were relatively well internally mixed. However, the BC presented a remarkably
200 different pattern with a much broader distribution and smaller peak sizes than its coating species, and
201 in particular, relatively small particles tended to have thin coatings.

202 Figs. 3b-f further present image plots of size distributions of the major aerosol components as a
203 function of R_{BC} (as a surrogate for coating thickness). Different from the average data shown in Fig.
204 3a, the coating species can be roughly classified into two modes separated by R_{BC} of ~ 4.5 . Most sulfate
205 and nitrate concentrated at $R_{BC} > 4.5$ (Figs. 3b and 3c): Sulfate peaked in a narrow R_{BC} range of 5.5–6.5,
206 while significant nitrate mass could distribute across a wider R_{BC} range (even to R_{BC} of ~ 8). Only
207 organics and chloride had a significant portion of mass distributed on relatively thinly coated BC-
208 containing particles at $R_{BC} < 4.5$ (Figs. 3e and 3f). Specifically, they both showed a sub-mode locating
209 in the regime with R_{BC} of ~ 3.5 –4.5 and D_{va} of ~ 200 –700nm. These sub-modes suggest that organics or
210 chloride are partially from primary sources as freshly emitted BC are more likely thinly coated. This
211 is consistent with that organics included species from fossil fuel and biomass burning combustion
212 revealed by the PMF analysis. Similarly, coal burning might contribute to chloride during wintertime
213 in Beijing (Sun et al., 2016). As for sulfate and nitrate, since they are predominantly secondary species,
214 they would coat on BC cores due to chemical aging therefore mostly distributed at higher R_{BC} .

215

216 3.3 Sources of organic coating species

217 The high-resolution mass spectra (HRMS) of different factors of the organic coating resolved from
218 PMF analyses, their relative contributions and diurnal cycles of temporal variations relative to BC are
219 shown in Fig. 4. Fig. 4a illustrates the mass profile of the fossil fuel combustion OA with BC carbon
220 clusters (FFOA + BC). This factor had a low O/C ratio of 0.16. In this work, this factor might include
221 emissions from both traffic and coal combustion, as it contained a series of significant PAHs ion
222 fragments in the mass spectrum (PAHs fragments are negligible in other factors) indicative of coal
223 burning (Sun et al., 2014; Sun et al., 2016), and presented a good correlation with $C_4H_9^+$ (r^2 of 0.72)
224 which is a AMS tracer ion of vehicle emissions (Zhang et al., 2005). Temporal variations of FFOA also
225 correlated well with $C_9H_7^+$ (m/z 115, r^2 of 0.92) and Cl^- (r^2 of 0.60), which have been proposed as
226 possible coal combustion tracer species (Yan et al., 2018; Sun et al., 2014). The FFOA/BC (Fig. 4f)
227 appeared to be higher during nighttime than that during daytime. Note the diurnal pattern of BC itself
228 (Fig. 5c) was similar as that of FFOA/BC. The diurnal variations of BC might be influenced by both



229 fossil fuel combustion activities and relatively low PBLH during nighttime. The fossil fuel combustion
230 included coal burning and vehicle emissions (gasoline cars, and the heavy-duty diesel vehicles that are
231 only allowed to enter the city during later night). The mass ratios of different factors to BC shall have
232 less influences from PBLH, therefore high levels of FFOA/BC strongly indicate that co-emitted
233 organic species with BC from fossil fuel combustion were enhanced during nighttime.

234 Figure 4b shows the mass spectrum of BBOA and related BC clusters. One feature of this factor
235 is that it had relatively high fractional contributions of $C_2H_4O_2^+$ (1.47% of total) and $C_3H_5O_2^+$ (0.95%),
236 which are often regarded as AMS marker ions from biomass burning emitted levoglucosan (Cubison
237 et al., 2011; Mohr et al., 2009). Note the FFOA also contained appreciable $C_2H_4O_2^+$ and $C_3H_5O_2^+$
238 signals, partially due to that coal burning (such as lignite) can emit some levoglucosan as well (Yan et
239 al., 2018). Nevertheless, mass fractions of $C_2H_4O_2^+$ and $C_3H_5O_2^+$ in FFOA were less than those in
240 BBOA, and they correlated much better with BBOA than those with FFOA (for examples, r^2 of 0.90
241 for BBOA vs. $C_2H_4O_2^+$, and 0.72 for FFOA vs. $C_2H_4O_2^+$). The BBOA correlated very well with another
242 biomass burning tracer - K^+ (r^2 of 0.90). In addition, BBOA had negligible PAHs ion fragments while
243 the FFOA contained remarkably high PAHs signals. Such characteristics are generally in agreement
244 with previous AMS findings in the same location during wintertime in Beijing (Sun et al., 2016). For
245 these reasons, the second factor was identified as BBOA. The diurnal pattern of BBOA/BC reached
246 minimum during afternoon and was overall high during nighttime, similar as FFOA/BC, indicating the
247 nighttime enhancement of BB-related organics emissions in wintertime Beijing.

248 Besides the two POA factors, we also identified two secondary OA factors (OOA1 and OOA2),
249 whose O/C ratios were 0.45 and 0.28, respectively. OOA1 was the most oxidized OA factor that had a
250 higher $CO_2^+/C_2H_3O^+$ ratio than that of OOA2. The correlation between OOA1 and sulfate was better
251 than it with nitrate (r^2 of 0.99 vs. 0.86). As a comparison, the less oxygenated OOA2 correlated better
252 with nitrate than it with sulfate (r^2 of 0.59 vs. 0.34). These characteristics are consistent with previous
253 AMS-PMF results (Zhang et al., 2011). Opposite to the diurnal cycles of FFOA and BBOA, the
254 OOA2/BC ratio arose significantly from early morning and peaked in the afternoon (~3pm). The
255 diurnal pattern of OOA1/BC presented a similar peak at ~3pm. This result demonstrates a clear
256 evidence and important role of photochemical reactions to the formation of secondary organic species.
257 However, the precursors leading to the formations of OOA1 and OOA2 remain to be elucidated.
258 Interestingly, for OOA1/BC, in addition to the peak during afternoon, the ratio increased during early



259 evening and remained at high levels until early morning. This result indicates that nighttime aqueous-
260 phase processing (high levels of RH during nighttime shown in Fig. 5a) can also contribute to OOA1
261 production. As such behavior was not observed for OOA2/BC, it agrees with previous field and
262 laboratory findings that aqueous-phase reactions tend to produce more highly oxygenated species
263 (Ervens et al., 2011; Ge et al., 2012; Herrmann et al., 2015; Xu et al., 2017).

264 Overall, the mass fractions of BC cores that were associated with fossil fuel combustion, biomass
265 burning, less and more oxygenated secondary processes were 32.7%, 31.8%, 18.7% and 16.9%,
266 respectively (Fig. 4e). The BC was predominantly coated by primary species.

267

268 3.4. Diurnal patterns of BC and coating species

269 Fig. 5 presents the diurnal cycles of meteorological parameters (T, RH, WS and WD), BC
270 concentrations and R_{BC} , mass ratios of major species to BC, gaseous species (CO, SO₂ and NO_x), O/C
271 and OS_c (oxidation state, defined as $2 \cdot O/C-H/C$) (Kroll et al., 2011). Note BC did not present a peak
272 at 8:00 am, yet R_{BC} , Org/BC, SO₄²⁻/BC, NO₃⁻/BC and Cl⁻/BC were all low at ~8:00 am. This was likely
273 attributed to increase of the mass fractions of fresh and barely coated BC-containing particles (rather
274 than the increase of absolute concentrations of fresh BC-containing particles) emitted during morning
275 rush hours from traffic emissions, etc. This was consistent with the decreases of O/C and OS_c and
276 increases of CO and NO₂ at 8:00 am of the day. On the contrary, the R_{BC} drop at ~4:00 pm was unlikely
277 due to influences of afternoon rush hours, as there were no increases of CO, NO₂, and both O/C and
278 OS_c were at high levels. In fact, the 4:00pm R_{BC} drop was mainly caused by the large decrease of
279 organics coating concentration - mainly fossil fuel and biomass burning OA (Fig. 4f).

280 The diurnal variation of NO₃⁻/BC peaked at ~3-4 pm, consistent with the variation of T, and similar
281 as those in the previous reports during wintertime in Beijing (Ge et al., 2017a; Sun et al., 2016),
282 reflecting the dominated contribution of photochemical formation of nitrate. SO₄²⁻/BC showed a
283 relatively small afternoon increase, indicating partial sulfate was produced from photochemical
284 activities; it also presented a nighttime enhancement, similar as OOA1/BC, suggesting the sulfate
285 formation in aqueous-phase, consistent with the nighttime increase of RH and decrease of temperature
286 (Fig. 5a). Due to increases of FFOA/BC, BBOA/BC and OOA1/BC (the portion likely from aqueous-
287 phase production), Org/BC remained at high levels during nighttime. All these increases added together,
288 leading to the high R_{BC} during nighttime. In addition, Cl⁻/BC varied generally similar to those of



289 FFOA/BC and BBOA/BC, again indicating its strong association with primary emissions.

290

291 **3.5 Characteristics of coating species during different periods**

292 **3.5.1 Coating compositions at clean and pollution periods**

293 Fig. 6 shows the variations of BC-coating compositions as a function of coating thickness during
294 clean (CP) and pollution periods (PP) (separated by the concentration of $10 \mu\text{g}/\text{m}^3$), respectively.
295 Contrasting difference of the coating composition during these two cases was observed: primary OA
296 (especially FFOA) appeared to be the most abundant component during CP while mass contributions
297 of secondary organic and inorganic species were remarkably high during PP (Figs. 6a and b), and the
298 average R_{BC} during PP (~ 5.1) was also higher than that during CP (~ 4.5) (Fig. 6f). These results again
299 reinforce the importance of secondarily formed species to the heavy haze pollution in urban Beijing
300 (Huang et al., 2014). Furthermore, the BC coating composition as well as OS_c during CP were both
301 relatively stable against R_{BC} (Fig. 6c). On the contrary, during PP, with the increase of R_{BC} , the mass
302 fractions of secondary species (OOA1, nitrate and sulfate) increased clearly, especially at $R_{\text{BC}} > 5$;
303 consistently, OS_c of organic coating increased from ~ -0.85 to > -0.70 . Such behavior again highlights
304 the contribution of chemical aging process to the heavy haze pollution.

305 Relative to other observations (Wang et al., 2017a; Massoli et al., 2015; Cappa et al., 2012), the
306 levels of R_{BC} during both CP and PP are much smaller than those for highly aged BC, which might
307 have $R_{\text{BC}} > 10$. This can be expected for urban aerosols. On the other hand, the R_{BC} levels here are also
308 generally higher than those found for the BC-containing particles in Los Angeles where the average
309 R_{BC} was typically smaller than 4 due to predominant influence of vehicle emissions (Lee et al., 2017).
310 Regarding the variations of coating composition vs. R_{BC} , the behavior during PP is in fact consistent
311 with a few previous field measurement results in American or European urban locations (Massoli et
312 al., 2015; Liu et al., 2017; Lee et al., 2017; Cappa et al., 2012; Collier et al., 2018), indicating a general
313 behavior for BC-containing particles in urban area that more aged BC tends to have thicker coating.
314 Yet this property can be altered if significant POA emissions exist, such as the case during CP in this
315 work, and a case with heavy BBOA influences observed in Tibet Plateau (Wang et al., 2017a).

316

317 **3.5.2 Coating compositions at two different episodes**

318 Although we demonstrated in Section 3.5.1, the heavy pollution of BC-containing particles was



319 on average associated with more secondary species, the underlying governing factors of individual
320 pollution events might vary from each other. Here we investigated the characteristics of BC-containing
321 particles in two most polluted episodes occurring during the campaign. The first episode (FE) was
322 accompanied with relatively high RH (from 6:00 pm of 3 Dec. to 8:00 am of 4 Dec., 2016), while the
323 second episode (SE) was dominated by primary emissions (from 0:00 am to 6:00 am of 11 Dec., 2016).
324 The average mass loadings of BC cores and BC-containing particles were $18.1 \mu\text{g m}^{-3}$ and $123.1 \mu\text{g m}^{-3}$
325 m^{-3} during FE, $14.4 \mu\text{g m}^{-3}$ and $80.0 \mu\text{g m}^{-3}$ during SE, respectively - both were much higher than the
326 campaign-averaged BC of $4.9 \mu\text{g m}^{-3}$ and BC-containing particles of $29.4 \mu\text{g m}^{-3}$.

327 For FE, the average T and RH were $\sim 4.2^\circ\text{C}$ and $\sim 78\%$, respectively. The average T was close to
328 the campaign-average value of 4.8°C , but the air was more humid than the campaign-average RH of
329 $\sim 50\%$. Correspondingly, we observed clear increases of the mass contributions of sulfate from 6.5%
330 to 10.3%, nitrate from 8.8% to 10.2%, OOA1 from 7.5% to 11.5% (Figs. 7a and 7c). Such
331 enhancements were very likely linked with the aqueous-phase processing as this episode occurred
332 during nighttime and was characterized with high RH conditions. During FE, nitrate and sulfate also
333 correlated very well (r^2 of 0.94; Fig. S4), therefore formation of nitrate would also relate with aqueous-
334 phase processing in this episode. As a comparison, the mass fraction of photochemical-relevant OOA2
335 decreased significantly from campaign-average 13.3% to 9.8%. In addition, mass fraction of Cl^- also
336 increased from campaign-average 4.0% to 5.3%; meanwhile, we found that relative to the campaign-
337 average values, the KCl^+/BC ratio decreased 14%, the $\text{K}_3\text{SO}_4^+/\text{BC}$ ratio increased 28%, possibly
338 indicating that the heterogeneous replacement reactions of coal-burning related Cl^- by SO_4^{2-} during FE
339 (Fig. S4). Overall, due to mainly the aqueous-phase production of secondary coating components,
340 comparing to campaign-average values, the average R_{BC} during FE became larger (5.5 vs. 5.0), the OA
341 became more oxygenated (O/C of 0.18 vs. 0.15), and size distributions of OA, sulfate and nitrate all
342 shifted to larger peak sizes (Fig. S5a).

343 On the other hand, for SE, even though it also occurred during nighttime, the average RH was
344 significantly low ($\sim 47\%$), and it was overwhelmingly dominated by primary species (50.6% of FFOA,
345 15.2% of BBOA and 18% of BC). Secondary sulfate and nitrate only occupied 2.5% and 2.2% of the
346 total mass of BC-containing particles. Nighttime aqueous-phase related OOA1 contribution was nearly
347 negligible (only 0.8%), which in another way, manifests that nighttime efficient OOA1 production was
348 strongly associated with high RH conditions. Due to the contribution of fresh primary emissions, the



349 coating OA was less oxygenated than that of campaign-averaged OA (O/C of 0.12 vs. 0.15), and the
350 average R_{BC} during PE was consistently smaller (4.5 vs. 5.0). Mass spectrum of BC-Org (Fig. 7b) also
351 contained significant PAHs fragments, in line with the large contribution from FFOA (mainly coal
352 combustion). Average size distribution of OA during SE was broader and peaked in a smaller diameter
353 (<500 nm D_{va}) (Fig. S5b), in response to the dominance of POA. Occurrence of the highly polluted SE
354 demonstrates that even though the pollutions of BC-containing particles in urban Beijing during winter
355 are on average governed by secondary species, local primary emissions sometimes can lead to serious
356 and short-term pollution events as well.

357

358 4. Conclusions

359 As part of the UK-China 2016 APHH winter campaign, for the first time, an Aerodyne SP-AMS
360 was introduced to exclusively determine the chemical compositions of BC-containing particles in
361 urban Beijing. We found the average concentrations of BC and its coating species were 4.9 and 24.5
362 $\mu\text{g m}^{-3}$, namely the R_{BC} (mass ratio of coating to BC) was ~ 5.0 . The coating was dominated by organics
363 (59.4% of total mass of BC-containing particles), followed by nitrate and sulfate (15.3% together).
364 Size distribution data demonstrate that larger BC-containing particles tend to have thicker coating,
365 more secondary species and more internally mixed coating components. PMF analyses further
366 identified two POA factors related with fossil fuel and biomass burning, respectively, which dominated
367 the total OA mass. Two SOA factors were also separated, and both of them were found to be mainly
368 contributed by photochemical activities, besides a fraction of the highly oxidized OA factor could be
369 produced by nighttime aqueous-phase reactions. In addition, significant photochemical formation of
370 nitrate rather than sulfate was observed.

371 Comparisons of the coating compositions between clean and pollution periods shows the critically
372 important role of chemical aging for the pollution of BC-containing particles in urban Beijing. We also
373 found that in one case, aqueous-phase production might lead to serious pollution under high RH
374 conditions, while in another case, fossil fuel combustion could cause extreme and short-term heavy
375 pollution. Comparisons between the BC-containing particles and the total submicron aerosol particles
376 during this campaign will be presented in details in near future.

377

378 Acknowledgements



379 This work was supported by the National Key R&D program of China (2016YFC0203501), the
380 Natural Science Foundation of China (21777073, 91544220, 21577065, and 41571130034), and the
381 International ST Cooperation Program of China (2014DFA90780), the UK Natural Environment
382 Research Council (grant ref. NE/N00695X/1).

383

384 **References**

- 385 Aiken, A. C., Decarlo, P. F., Kroll, J. H., Worsnop, D. R., Huffman, J. A., Docherty, K. S., Ulbrich, I. M., Mohr, C., Kimmel,
386 J. R., Sueper, D., Sun, Y., Zhang, Q., Trimborn, A., Northway, M., Ziemann, P. J., Canagaratna, M. R., Onasch, T. B.,
387 Alfarra, M. R., Prevot, A. S. H., Dommen, J., Duplissy, J., Metzger, A., Baltensperger, U., and Jimenez, J. L.: O/C and
388 OM/OC ratios of primary, secondary, and ambient organic aerosols with high-resolution time-of-flight aerosol mass
389 spectrometry, *Environ. Sci. Tech.*, 42, 4478-4485, 2008.
- 390 Bond, T. C., Doherty, S. J., Fahey, D. W., Forster, P. M., Berntsen, T., DeAngelo, B. J., Flanner, M. G., Ghan, S., Kärcher,
391 B., Koch, D., Kinne, S., Kondo, Y., Quinn, P. K., Sarofim, M. C., Schultz, M. G., Schulz, M., Venkataraman, C.,
392 Zhang, H., Zhang, S., Bellouin, N., Guttikunda, S. K., Hopke, P. K., Jacobson, M. Z., Kaiser, J. W., Klimont, Z.,
393 Lohmann, U., Schwarz, J. P., Shindell, D., Storelvmo, T., Warren, S. G., and Zender, C. S.: Bounding the role of black
394 carbon in the climate system: A scientific assessment, *J. Geophys. Res.-Atmos.*, 118, 5380-5552, 2013.
- 395 Canagaratna, M. R., Jayne, J. T., Jimenez, J. L., Allan, J. D., Alfarra, M. R., Zhang, Q., Onasch, T. B., Drewnick, F., Coe,
396 H., Middlebrook, A., Delia, A., Williams, L. R., Trimborn, A. M., Northway, M. J., DeCarlo, P. F., Kolb, C. E.,
397 Davidovits, P., and Worsnop, D. R.: Chemical and microphysical characterization of ambient aerosols with the
398 aerodyne aerosol mass spectrometer, *Mass Spectrom. Rev.*, 26, 185-222, 2007.
- 399 Canagaratna, M. R., Massoli, P., Browne, E. C., Franklin, J. P., Wilson, K. R., Onasch, T. B., Kirchstetter, T. W., Fortner,
400 E. C., Kolb, C. E., Jayne, J. T., Kroll, J. H., and Worsnop, D. R.: Chemical compositions of black carbon particle cores
401 and coatings via soot particle aerosol mass spectrometry with photoionization and electron ionization, *J. Phys. Chem.*
402 *A*, 119, 4589-4599, 2015.
- 403 Cappa, C. D., Onasch, T. B., Massoli, P., Worsnop, D. R., Bates, T. S., Cross, E. S., Davidovits, P., Hakala, J., Hayden, K.
404 L., Jobson, B. T., Kolesar, K. R., Lack, D. A., Lerner, B. M., Li, S.-M., Mellon, D., Nuaaman, I., Olfert, J. S., Petäjä,
405 T., Quinn, P. K., Song, C., Subramanian, R., Williams, E. J., and Zaveri, R. A.: Radiative absorption enhancements
406 due to the mixing state of atmospheric black carbon, *Science*, 337, 1078-1081, 2012.
- 407 Chen, C., Fan, X., Shaltout, T., Qiu, C., Ma, Y., Goldman, A., and Khalizov, A. F.: An unexpected restructuring of
408 combustion soot aggregates by subnanometer coatings of polycyclic aromatic hydrocarbons, *Geophys. Res. Lett.*, 43,
409 11080-11088, 2016a.
- 410 Chen, Y., Schleicher, N., Fricker, M., Cen, K., Liu, X.-l., Kaminski, U., Yu, Y., Wu, X., and Norra, S.: Long-term variation
411 of black carbon and PM_{2.5} in Beijing, China with respect to meteorological conditions and governmental measures,
412 *Environ. Pollut.*, 212, 269-278, 2016b.
- 413 Cheng, Y., He, K.-b., Engling, G., Weber, R., Liu, J., Du, Z.-y., and Dong, S.-p.: Brown and black carbon in Beijing aerosol:
414 Implications for the effects of brown coating on light absorption by black carbon, *Sci. Total. Environ.*, 599-600, 1047-
415 1055, 2017.
- 416 Collier, S., Williams, L. R., Onasch, T. B., Cappa, C. D., Zhang, X., Russell, L. M., Chen, C.-L., Sanchez, K. J., Worsnop,
417 D. R., and Zhang, Q.: Influence of emissions and aqueous processing on particles containing black carbon in a polluted
418 urban environment: insights from a soot particle-aerosol mass spectrometer, *J. Geophys. Res.-Atmos.*, 123, 6648-
419 6666, 2018.
- 420 Cubison, M. J., Ortega, A. M., Hayes, P. L., Farmer, D. K., Day, D., Lechner, M. J., Brune, W. H., Apel, E., Diskin, G. S.,



- 421 Fisher, J. A., Fuelberg, H. E., Hecobian, A., Knapp, D. J., Mikoviny, T., Riemer, D., Sachse, G. W., Sessions, W.,
422 Weber, R. J., Weinheimer, A. J., Wisthaler, A., and Jimenez, J. L.: Effects of aging on organic aerosol from open
423 biomass burning smoke in aircraft and laboratory studies, *Atmos. Chem. Phys.*, 11, 12049-12064, 2011.
- 424 Cui, X., Wang, X., Yang, L., Chen, B., Chen, J., Andersson, A., and Gustafsson, Ö.: Radiative absorption enhancement
425 from coatings on black carbon aerosols, *Sci. Total Environ.*, 551–552, 51-56, 2016.
- 426 Ding, A. J., Huang, X., Nie, W., Sun, J. N., Kerminen, V. M., Petäjä, T., Su, H., Cheng, Y. F., Yang, X. Q., Wang, M. H.,
427 Chi, X. G., Wang, J. P., Virkkula, A., Guo, W. D., Yuan, J., Wang, S. Y., Zhang, R. J., Wu, Y. F., Song, Y., Zhu, T.,
428 Zilitinkevich, S., Kulmala, M., and Fu, C. B.: Enhanced haze pollution by black carbon in megacities in China,
429 *Geophys. Res. Lett.*, 43, 2873-2879, 2016.
- 430 Dusek, U., Reischl, G. P., and Hitzenberger, R.: CCN activation of pure and coated carbon black particles, *Environ. Sci.*
431 *Tech.*, 40, 1223-1230, 2006.
- 432 Dusek, U., Frank, G. P., Curtius, J., Drewnick, F., Schneider, J., Kurten, A., Rose, D., Andreae, M. O., Borrmann, S., and
433 Poschl, U.: Enhanced organic mass fraction and decreased hygroscopicity of cloud condensation nuclei (CCN) during
434 new particle formation events, *Geophys. Res. Lett.*, 37 (3) :174-180, 2010.
- 435 Ervens, B., Turpin, B. J., and Weber, R. J.: Secondary organic aerosol formation in cloud droplets and aqueous particles
436 (aqSOA): a review of laboratory, field and model studies, *Atmos. Chem. Phys.*, 11, 22301-22383, 2011.
- 437 Ge, X., Zhang, Q., Sun, Y., Ruehl, C. R., and Setyan, A.: Effect of aqueous-phase processing on aerosol chemistry and size
438 distributions in Fresno, California, during wintertime, *Environ. Chem.*, 9, 221-235, 2012.
- 439 Ge, X., He, Y., Sun, Y., Xu, J., Wang, J., Shen, Y., and Chen, M.: Characteristics and formation mechanisms of fine
440 particulate nitrate in typical urban areas in china, *Atmosphere*, 8, 62, 2017a.
- 441 Ge, X., Li, L., Chen, Y., Chen, H., Wu, D., Wang, J., Xie, X., Ge, S., Ye, Z., Xu, J., and Chen, M.: Aerosol characteristics
442 and sources in Yangzhou, China resolved by offline aerosol mass spectrometry and other techniques, *Environ. Pollut.*,
443 225, 74-85, 2017b.
- 444 Herrmann, H., Schaefer, T., Tilgner, A., Styler, S. A., Weller, C., Teich, M., and Otto, T.: Tropospheric aqueous-phase
445 chemistry: kinetics, mechanisms, and its coupling to a changing gas phase, *Chem. Rev.*, 115, 4259, 2015.
- 446 Huang, R.-J., Zhang, Y., Bozzetti, C., Ho, K.-F., Cao, J.-J., Han, Y., Daellenbach, K. R., Slowik, J. G., Platt, S. M., Canonaco,
447 F., Zotter, P., Wolf, R., Pieber, S. M., Bruns, E. A., Crippa, M., Ciarelli, G., Piazzalunga, A., Schwikowski, M.,
448 Abbaszade, G., Schnelle-Kreis, J., Zimmermann, R., An, Z., Szidat, S., Baltensperger, U., Haddad, I. E., and Prévôt,
449 A. S. H.: High secondary aerosol contribution to particulate pollution during haze events in China, *Nature*, 514, 218-
450 222, 2014.
- 451 Jacobson, M. Z.: Strong radiative heating due to the mixing state of black carbon in atmospheric aerosols. *Nature*, 409,
452 695–697, 2001.
- 453 Jayne, J. T., Leard, D. C., Zhang, X., Davidovits, P., Smith, K. A., Kolb, C. E., and Worsnop, D. R.: Development of an
454 aerosol mass spectrometer for size and composition analysis of submicron particles, *Aerosol Sci. Tech.*, 33, 49 - 70,
455 2000.
- 456 Ji, D., Li, L., Pang, B., Xue, P., Wang, L., Wu, Y., Zhang, H., and Wang, Y.: Characterization of black carbon in an urban-
457 rural fringe area of Beijing, *Environ. Pollut.*, 223, 524-534, 2017.
- 458 Kroll, J.H., Donahue, N.M., Jimenez, J.L., Kessler, S.H., Canagaratna, M.R., Wilson, K.R., Altieri, K.E., Mazzoleni, L.R.,
459 Wozniak, A.S., Bluhm, H., Mysak, E.R., Smith, J.D., Kolb, C.E., Worsnop, D.R.: Carbon oxidation state as a metric
460 for describing the chemistry of atmospheric organic aerosol. *Nat. Chem.* 3, 133-139, 2011.
- 461 Laborde, M., Schnaiter, M., Linke, C., Saathoff, H., Naumann, K., Möhler, O., Berlenz, S., Wagner, U., Taylor, J., and Liu,
462 D.: Single particle soot photometer intercomparison at the AIDA chamber, *Atmos. Meas. Tech.*, 5, 3077-3097, 2012.
- 463 Lee, A. K. Y., Willis, M. D., Healy, R. M., Onasch, T. B., and Abbatt, J. P. D.: Mixing state of carbonaceous aerosol in an
464 urban environment: single particle characterization using the soot particle aerosol mass spectrometer (SP-AMS),



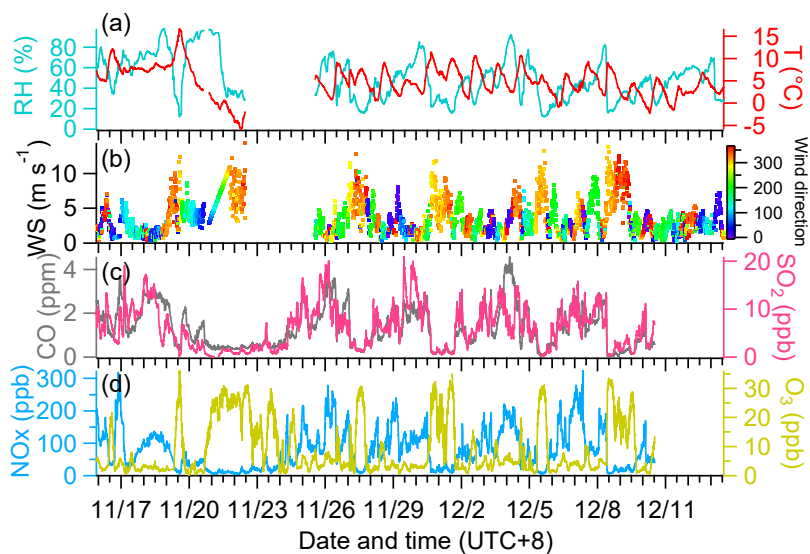
- 465 Atmos. Chem. Phys., 15, 1823-1841, 2015.
- 466 Lee, A. K. Y., Chen, C. L., Liu, J., Price, D. J., Betha, R., Russell, L. M., Zhang, X., and Cappa, C. D.: Formation of
467 secondary organic aerosol coating on black carbon particles near vehicular emissions, Atmos. Chem. Phys., 2017, 1-
468 20, 2017.
- 469 Liu, D., Allan, J., Whitehead, J., Young, D., Flynn, M., Coe, H., McFiggans, G., Fleming, Z. L., and Bandy, B.: Ambient
470 black carbon particle hygroscopic properties controlled by mixing state and composition, Atmos. Chem. Phys., 13,
471 2015-2029, 2013.
- 472 Liu, D., Whitehead, J., Alfarra, M. R., Reyes-Villegas, E., Spracklen, D. V., Reddington, C. L., Kong, S., Williams, P. I.,
473 Ting, Y.-C., Haslett, S., Taylor, J. W., Flynn, M. J., Morgan, W. T., McFiggans, G., Coe, H., and Allan, J. D.: Black-
474 carbon absorption enhancement in the atmosphere determined by particle mixing state, Nat. Geosci., 10, 184-188,
475 2017.
- 476 Liu, Q., Ma, T., Olson, M. R., Liu, Y., Zhang, T., Wu, Y., and Schauer, J. J.: Temporal variations of black carbon during
477 haze and non-haze days in Beijing, Sci. Rep., 6, 33331, 2016.
- 478 Liu, S., Aiken, A. C., Gorkowski, K., Dubey, M. K., Cappa, C. D., Williams, L. R., Herndon, S. C., Massoli, P., Fortner, E.
479 C., Chhabra, P. S., Brooks, W. A., Onasch, T. B., Jayne, J. T., Worsnop, D. R., China, S., Sharma, N., Mazzoleni, C.,
480 Xu, L., Ng, N. L., Liu, D., Allan, J. D., Lee, J. D., Fleming, Z. L., Mohr, C., Zotter, P., Szidat, S., and Prevot, A. S. H.:
481 Enhanced light absorption by mixed source black and brown carbon particles in UK winter, Nat. Commun., 6 :8435,
482 2015.
- 483 Massoli, P., Onasch, T. B., Cappa, C. D., Nuumaan, I., Hakala, J., Hayden, K., Li, S.-M., Sueper, D. T., Bates, T. S., Quinn,
484 P. K., Jayne, J. T., and Worsnop, D. R.: Characterization of black carbon-containing particles from soot particle aerosol
485 mass spectrometer measurements on the R/V Atlantis during CalNex 2010, J. Geophys. Res.-Atmos., 120,
486 2014JD022834, 2015.
- 487 Meng, J., Liu, J., Guo, S., Li, J., Li, Z., and Tao, S.: Trend and driving forces of Beijing's black carbon emissions from
488 sectoral perspectives, J. Clean. Prod., 112, 1272-1281, 2016.
- 489 Mohr, C., Huffman, J. A., Cubison, M. J., Aiken, A. C., Docherty, K. S., Kimmel, J. R., Ulbrich, I. M., Hannigan, M., and
490 Jimenez, J. L.: Characterization of primary organic aerosol emissions from meat cooking, trash burning, and motor
491 vehicles with high-resolution aerosol mass spectrometry and comparison with ambient and chamber observations,
492 Environ. Sci. Tech., 43, 2443-2449, 2009.
- 493 Onasch, T. B., Trimborn, A., Fortner, E. C., Jayne, J. T., Kok, G. L., Williams, L. R., Davidovits, P., and Worsnop, D. R.:
494 Soot particle aerosol mass spectrometer: development, validation, and initial application, Aerosol Sci. Tech., 46, 804-
495 817, 2012.
- 496 Paatero, P., and Tapper, U.: Positive matrix factorization: A non-negative factor model with optimal utilization of error
497 estimates of data values, Environmetrics, 5, 111-126, 1994.
- 498 Peng, J., Hu, M., Guo, S., Du, Z., Zheng, J., Shang, D., Levy, Z. M., Zeng, L., Shao, M., and Wu, Y. S.: Markedly enhanced
499 absorption and direct radiative forcing of black carbon under polluted urban environments, P Natl. Acad. Sci. USA,
500 113, 4266, 2016.
- 501 Pokhrel, R. P., Beamesderfer, E. R., Wagner, N. L., Langridge, J. M., Lack, D. A., Jayarathne, T., Stone, E. A., Stockwell,
502 C. E., Yokelson, R. J., and Murphy, S. M.: Relative importance of black carbon, brown carbon, and absorption
503 enhancement from clear coatings in biomass burning emissions, Atmos. Chem. Phys., 17, 5063-5078, 2017.
- 504 Ramanathan, V., and Carmichael, G.: Global and regional climate changes due to black carbon, Nat. Geosci, 1, 221-227,
505 2008.
- 506 Schleicher, N., Cen, K., and Norra, S.: Daily variations of black carbon and element concentrations of atmospheric particles
507 in the Beijing megacity – Part I: general temporal course and source identification, Chem Erde Geochem., 73, 51-60,
508 2013a.



- 509 Schleicher, N., Norra, S., Fricker, M., Kaminski, U., Chen, Y., Chai, F., Wang, S., Yu, Y., and Cen, K.: Spatio-temporal
510 variations of black carbon concentrations in the Megacity Beijing, *Environ. Pollut.*, 182, 392-401, 2013b.
- 511 Song, S., Wu, Y., Xu, J., Ohara, T., Hasegawa, S., Li, J., Yang, L., and Hao, J.: Black carbon at a roadside site in Beijing:
512 Temporal variations and relationships with carbon monoxide and particle number size distribution, *Atmos. Environ.*,
513 77, 213-221, 2013.
- 514 Sun, Y., Jiang, Q., Wang, Z., Fu, P., Li, J., Yang, T., and Yin, Y.: Investigation of the sources and evolution processes of
515 severe haze pollution in Beijing in January 2013, *J Geophys. Res.-Atmos.*, 119, 4380-4398, 2014.
- 516 Sun, Y., Du, W., Fu, P., Wang, Q., Li, J., Ge, X., Zhang, Q., Zhu, C., Ren, L., Xu, W., Zhao, J., Han, T., Worsnop, D. R.,
517 and Wang, Z.: Primary and secondary aerosols in Beijing in winter: sources, variations and processes, *Atmos. Chem.*
518 *Phys.*, 16, 8309-8329, 2016.
- 519 Sun, Y., Zhang, Q., Schwab, J. J., Yang, T., Ng, N. L., and Demerjian, K. L.: Factor analysis of combined organic and
520 inorganic aerosol mass spectra from high resolution aerosol mass spectrometer measurements, *Atmos. Chem. Phys.*,
521 12, 8537-8551, 2012.
- 522 Ulbrich, I. M., Canagaratna, M. R., Zhang, Q., Worsnop, D. R., and Jimenez, J. L.: Interpretation of organic components
523 from Positive Matrix Factorization of aerosol mass spectrometric data, *Atmos. Chem. Phys.*, 9, 2891-2918, 2009.
- 524 Wang, J., Onasch, T. B., Ge, X., Collier, S., Zhang, Q., Sun, Y., Yu, H., Chen, M., Prévôt, A. S. H., and Worsnop, D. R.:
525 Observation of fullerene soot in eastern China, *Environ. Sci. Tech. Lett.*, 3, 121-126, 2016a.
- 526 Wang, J., Zhang, Q., Chen, M.-D., Collier, S., Zhou, S., Ge, X., Xu, J., Shi, J., Xie, C., Hu, J., Ge, S., Sun, Y., and Coe, H.:
527 First chemical characterization of refractory black carbon aerosols and associated coatings over the Tibetan Plateau
528 (4730 m a.s.l), *Environ. Sci. Tech.*, 51 (24) :14072, 2017a.
- 529 Wang, J., Wu, Y., Ge, X., Shen, Y., Ge, S., Chen, M.: Characteristics and sources of ambient refractory black carbon aerosols:
530 Insights from soot particle aerosol mass spectrometer. *Atmos. Environ.*, 185, 147-152, 2018.
- 531 Wang, Q., Huang, R.-J., Cao, J., Tie, X., Shen, Z., Zhao, S., Han, Y., Li, G., Li, Z., Ni, H., Zhou, Y., Wang, M., Chen, Y.,
532 and Su, X.: Contribution of regional transport to the black carbon aerosol during winter haze period in Beijing, *Atmos.*
533 *Environ.*, 132, 11-18, 2016b.
- 534 Wang, Y., de Foy, B., Schauer, J. J., Olson, M. R., Zhang, Y., Li, Z., and Zhang, Y.: Impacts of regional transport on black
535 carbon in Huairou, Beijing, China, *Environ. Pollut.*, 221, 75-84, 2017b.
- 536 Willis, M. D., Lee, A. K. Y., Onasch, T. B., Fortner, E. C., Williams, L. R., Lambe, A. T., Worsnop, D. R., and Abbatt, J. P.
537 D.: Collection efficiency of the Soot-Particle Aerosol Mass Spectrometer (SP-AMS) for internally mixed particulate
538 black carbon, *Atmos. Meas. Tech.*, 7, 5223-5249, 2014.
- 539 Willis, M. D., Healy, R. M., Riemer, N., West, M., Wang, J. M., Jeong, C. H., Wenger, J. C., Evans, G. J., Abbatt, J. P. D.,
540 and Lee, A. K. Y.: Quantification of black carbon mixing state from traffic: implications for aerosol optical properties,
541 *Atmos. Chem. Phys.*, 16, 4693-4706, 2016.
- 542 Wu, Y., Zhang, R., Tian, P., Tao, J., Hsu, S. C., Yan, P., Wang, Q., Cao, J., Zhang, X., and Xia, X.: Effect of ambient
543 humidity on the light absorption amplification of black carbon in Beijing during January 2013, *Atmos Environ.*, 124,
544 217-223, 2016.
- 545 Wu, Y., Wang, X., Tao, J., Huang, R., Tian, P., Cao, J., Zhang, L., Ho, K. F., Han, Z., and Zhang, R.: Size distribution and
546 source of black carbon aerosol in urban Beijing during winter haze episodes, *Atmos. Chem. Phys.*, 17, 7965-7975,
547 2017.
- 548 Xu, W., Han, T., Du, W., Wang, Q., Chen, C., Zhao, J., Zhang, Y., Li, J., Fu, P., Wang, Z., Worsnop, D. R., and Sun, Y.:
549 Effects of aqueous-phase and photochemical processing on secondary organic aerosol formation and evolution in
550 Beijing, China, *Environ. Sci. Tech.*, 51, 762-770, 2017.
- 551 Yan, C., Zheng, M., Sullivan, A. P., Shen, G., Chen, Y., Wang, S., Zhao, B., Cai, S., Desyaterik, Y., Li, X., Zhou, T.,
552 Gustafsson, Ö., and Collett, J. L.: Residential coal combustion as a source of levoglucosan in China, *Environ. Sci.*



- 553 Tech., 52, 1665-1674, 2018.
- 554 Yang, T., Guilin, H., and Zhifang, X.: Atmospheric Black Carbon Deposit in Beijing and Zhangbei, China, *Procedia Earth*
555 *and Planet. Sci.*, 10, 383-387, 2014.
- 556 Zhang, Q., Alfarra, M. R., Worsnop, D. R., Allan, J. D., Coe, H., Canagaratna, M. R., and Jimenez, J. L.: Deconvolution
557 and quantification of hydrocarbon-like and oxygenated organic aerosols based on aerosol mass spectrometry, *Environ.*
558 *Sci. Tech.*, 39, 4938-4952, 2005.
- 559 Zhang, Q., Jimenez, J., Canagaratna, M., Ulbrich, I., Ng, N., Worsnop, D., and Sun, Y.: Understanding atmospheric organic
560 aerosols via factor analysis of aerosol mass spectrometry: a review, *Anal. Bioanal. Chem.*, 401, 3045-3067, 2011.
- 561 Zhang, S., Wu, Y., Yan, H., Du, X., Max Zhang, K., Zheng, X., Fu, L., and Hao, J.: Black carbon pollution for a major road
562 in Beijing: Implications for policy interventions of the heavy-duty truck fleet, *Transport. Res. D-TR E*, 2017.
- 563



564

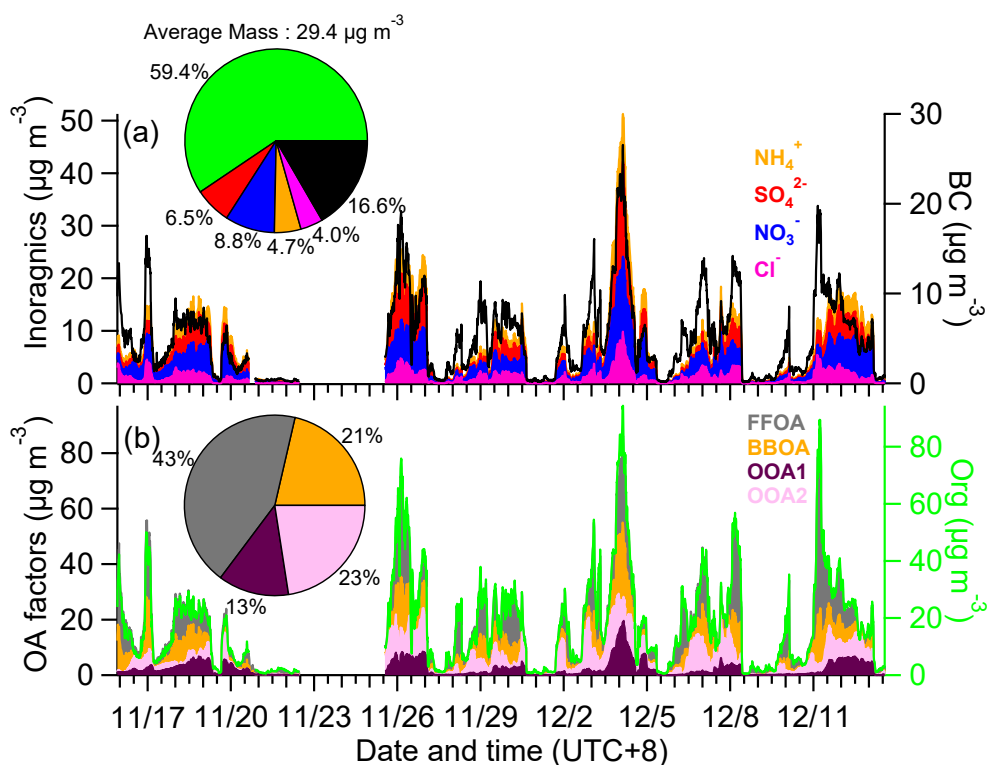
565 Figure 1. Temporal variation of (a) relative humidity (RH) and temperature (T, °C), (b) wind speed (WS, m s⁻¹) and wind

566 direction (WD), and (c)(d) mass loadings of CO, SO₂, NO_x and O₃.

567

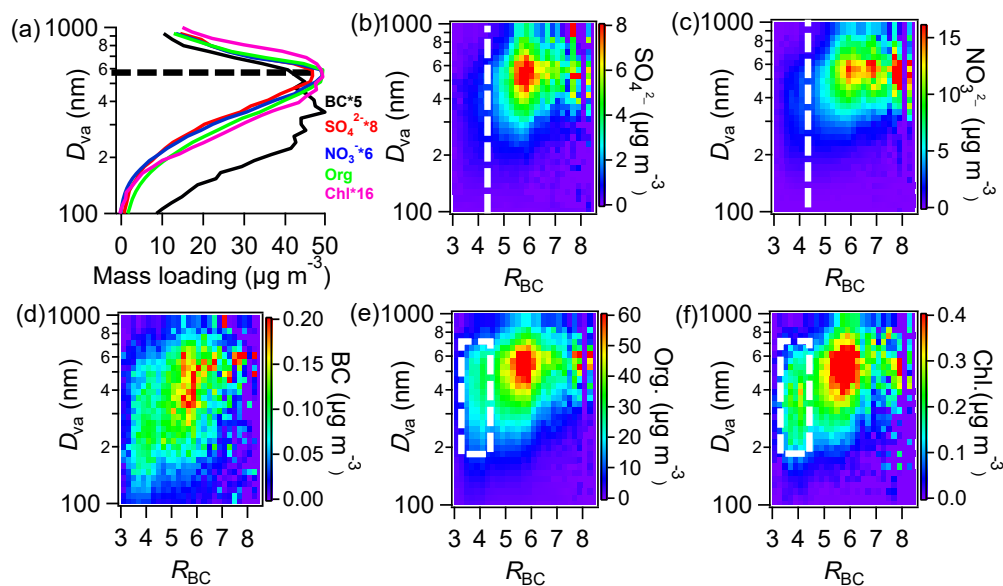


568



569

570 Figure 2. (a) Temporal variations of mass loadings of inorganic coating components (sulfate, nitrate, ammonium and
571 chloride) and BC cores, and (b) temporal variations of mass loadings of organic coating (Org) and PMF separated OA
572 factors (inset pie charts show the average composition of total BC-containing particles, and organics, respectively).
573



574

575

Figure 3. Mass-based campaign-averaged size distributions: (a) major coating components and BC cores, and (b-f) image

576

plots of size distributions of sulfate, nitrate, BC, organics, and chloride as a function of R_{BC} (mass ratio of coating-to-BC)

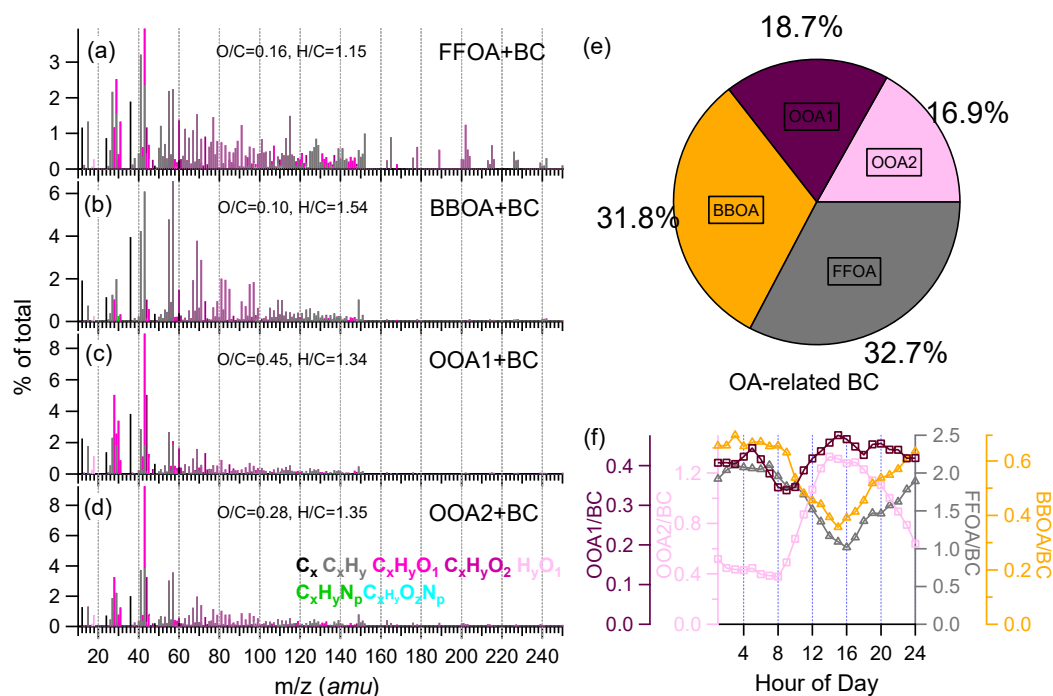
577

(Note size distributions of BC and chloride were scaled from those of m/z 24 and m/z 35, respectively)

578



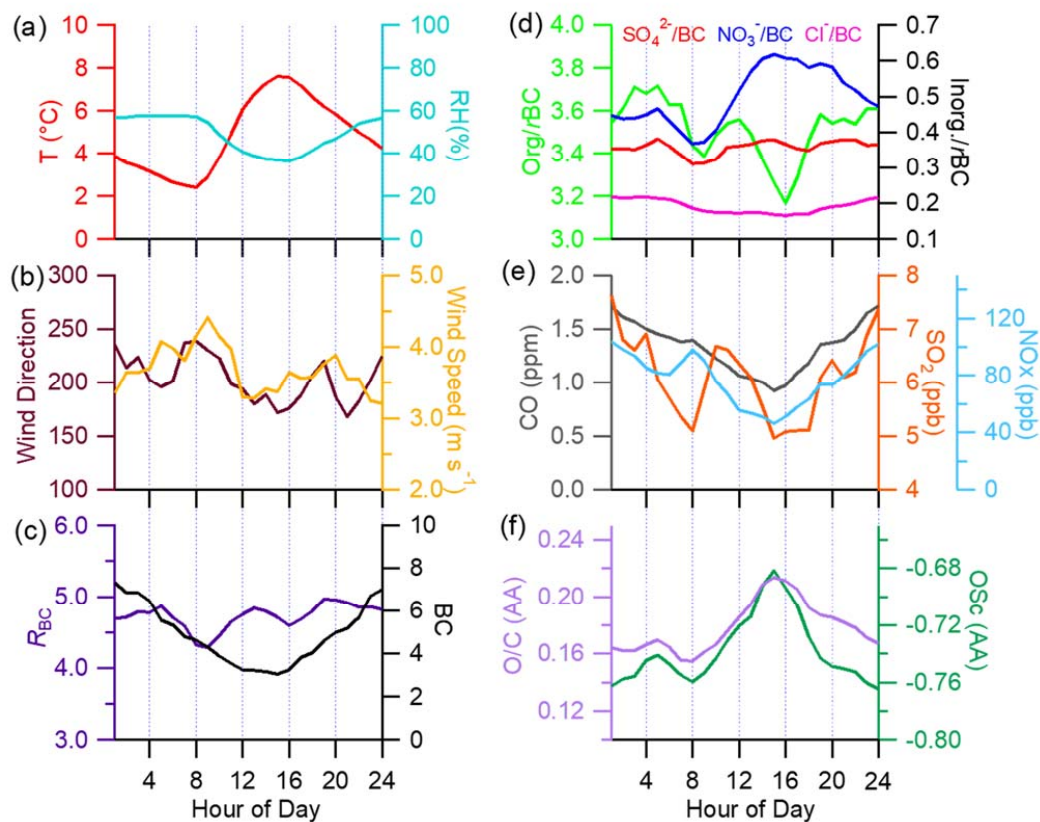
579



580

581 Figure 4. High-resolution mass spectra of (a) fossil fuel combustion OA (FFOA + BC), (b) biomass burning OA (BBOA +
 582 BC), (c) OOA1 + BC, (d) OOA2 + BC, (e) Mass fractions of the BC fragments apportioned in different OA factors, and (f)
 583 diurnal cycles of the four OA factors relative to BC.

584

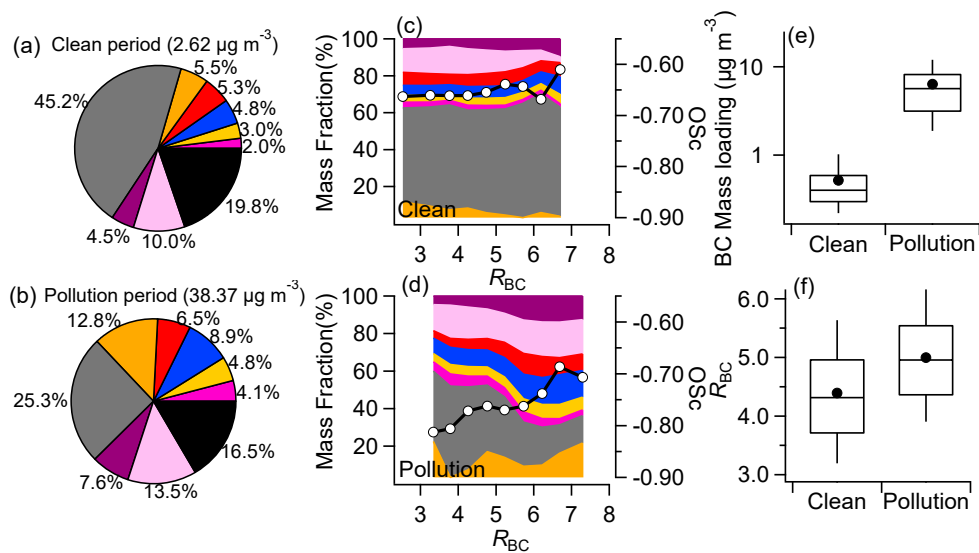


585

586 Figure 5. Diurnal cycles of (a) T and RH, (b) wind direction and wind speed, (c) mass ratio of coatings to BC (R_{BC}) and
587 BC, (d) Org/BC, SO_4^{2-}/BC , NO_3^-/BC and Cl^-/BC , (e) mass loading of gaseous species (CO, SO_2 , NO_x), and (f) O/C and
588 oxidation state ($OS_c=2*O/C-H/C$).
589



590

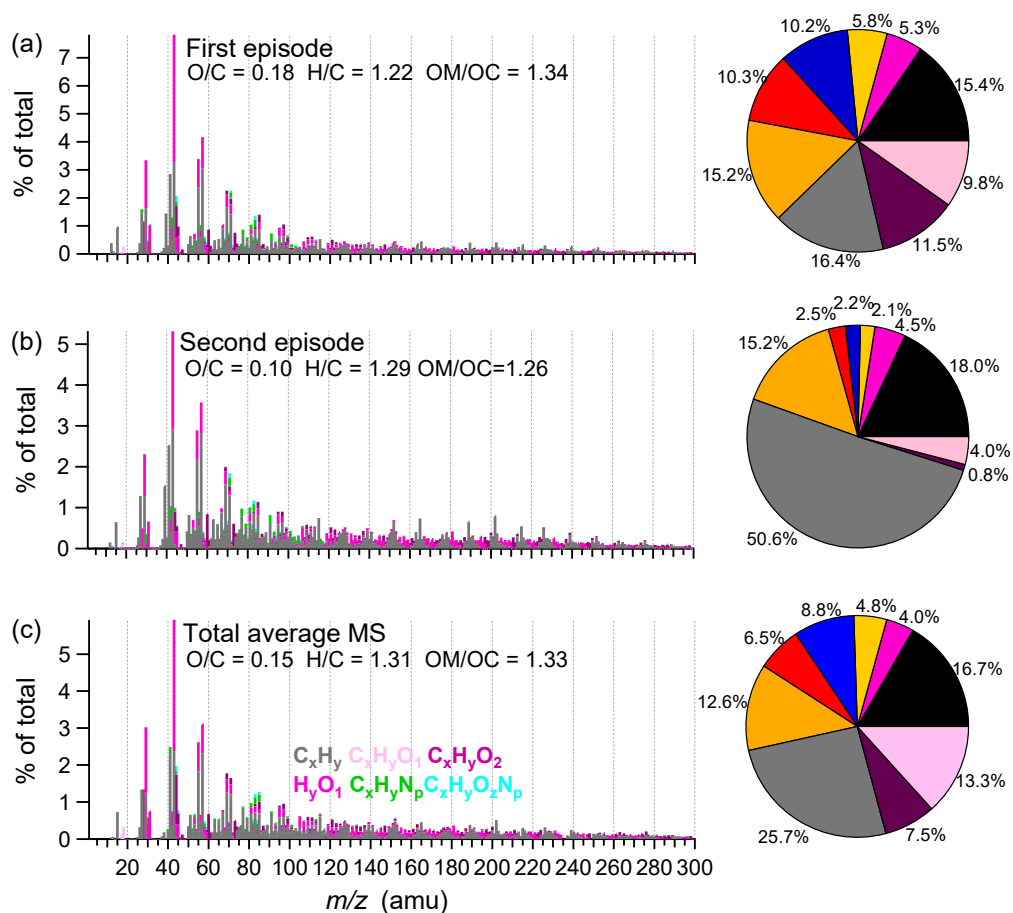


591

592 Figure 6. (a)(b) Average compositions of BC-containing particles during clean and pollution periods, (c)(d) mass fractions
 593 of the non-BC coating components (left y-axis) and OS_c (right y-axis) during clean and pollution periods as a function of
 594 R_{BC} , box plots of BC mass loadings (e) and R_{BC} during clean and pollution periods (colors of the components are consistent
 595 with those in Fig. 2).
 596



597



598

599 Figure 7. High-resolution mass spectra of the average OA at different episodes: (a) first episode (FE), (b) second episode
 600 (SE) and (c) whole campaign (inset pies show the average compositions during corresponding episodes; colors of
 601 different components are consistent with those in Fig. 2).

602

603

604